The influence of the structure of ultrafine-grained aluminium alloys on their mechanical properties under dynamic compression and shock-wave loading

I G Brodova[1], A N Petrova[1, 2], O B Naimark[3], O A Plekhov[3], S V Razorenov[4] and E V Shorokhov[5]

[1] M.N. Miheev Institute of Metal Physics of Ural Branch of Russian Academy of Sciences, 620990, 18 S. Kovalevskaya Street, Ekaterinburg, Russia
[2] Ural Federal University, 620002, 19 Mira street, Ekaterinburg, Russia
[3] Institute of Continuous Media Mechanics of the Ural Branch of Russian Academy of Science, 614013, 1 Academician Korolev Street, Perm, Russia
[4] Institute of Problems of Chemical Physics of Russian Academy of Sciences, 142432, 1 Academician Semenov Avenue, Chernogolovka, Moscow region, Russian Federation
[5] Federal State Unitary Enterprise "Russian Federal Nuclear Center – Academician E.I. Zababakhin All-Russian Research Institute of Technical Physics", 456770, 13 Vasiliev Street, PO box 245, Snezhinsk, Chelyabinsk region, Russia

E-mail: brodova@imp.uran.ru

Abstract. Mechanical properties of commercial A3003 and A7075 aluminum alloys having ultrafine-grained structure formed under dynamic channel angular pressing were investigated. It was shown that yield strength of ultrafine-grained alloys at the wide range of strain rates from 2 10^{-3} to 1.5 10^{5} s^{-1} are higher than of coarse-grained alloys. The values of dissipated energy ratio of the ultrafine-grained alloys were compared concerning their different structures and strain rate of 3.5-6.6 10^{3} s^{-1}. Under shock-wave loading the decreasing of strength was observed for both investigated UFG alloys against quasi-static deformation at the strain rate of 10^{3} s^{-1}.

1. Introduction

Industrial aluminum alloys are current and extensively used materials for different applications. For secure operation of constructions, high requirements are imposed on strength and plasticity of aluminum alloys. It is common knowledge that mechanical properties of aluminum alloys are governed by structure and their phase composition. In recent years, the various methods of severe plastic deformation are widely used for structural refinement of the metallic materials. Materials with the grain size below 1μmwere so named ultrafine-grained (UFG) materials. It was shown that UFG materials have advanced static mechanical properties in comparison with conventional coarse-grained materials. However, at high strain-rate deformation and shock wave loading this benefit decays or sometimes even disappears [1-7]. Experimental and theoretical researches indicated that at specified deformation conditions under shock wave loading the initial temperature effects on elastic-plastic

properties and a fracture behavior [2, 5, 6]. Thus, at the temperature about melting point the anomalous growth of an elastic precursor amplitude (approximately by four times) and sharp reduction of spall strength were demonstrated. Many researchers showed that deformation resistance and spall strength depend on grain size, type of the defects and their density [3, 5, 8, 9].Nevertheless, experimental data about strain rate dependence of mechanical properties of different aluminum alloys are quiet controversial and do not answer the questions about structural parameters contribution to deformation mechanisms at dynamic conditions.

The aim of the present study was systematical investigation of mechanical behavior of UFG aluminum alloys at the wide range of strain rates. The UFG alloys were produced by means of unique method of dynamic pressing. As it was shown [10-12] structure and mechanical properties of such alloys distinct from UFG alloys processed by static methods of severe plastic deformation. The studying of their behavior under shock wave conditions gives new knowledge about the character of phenomena in FCC metals.

2. Experimental

2.1. Material and processing

The rods of commercial A3003 (Al–1.5 Mn–0.1 Zn–0.05 Cu–0.6 Si–0.7 Fe in wt%) and A7075 (Al–7.0 Zn–2.3 Mg–1.8 Cu–0.5 Si–0.5 Fe–0.25 Cr in wt%) alloys having length of 75 mm and diameter of 16 mm were processed by the method of severe plastic deformation – Dynamic channel angular pressing (DCAP). Due to the action of powder gases pressure on the piston, the alloys were deformed with the strain rate of the order of 10^5 s^{-1}. The unique feature of the DCAP is the combination of a shock-wave loading and following high-strain rate shear deformation. The DCAP scheme is described in details in [10, 11]. DCAP provides grain refinement in the alloys to 200-500 nm. The A3003 alloy was deformed by 1 (DCAP-1) and 4 (DCAP-4) pressing cycles and the A7075 alloy was deformed by 2 pressing cycles (DCAP-2). Repeated deformation was performed using B_c route. Typical structures of DCAP alloys are shown in figure 1, 2.

After one pressing cycle the structure of A3003 alloy is composed by sells and subgrains with low-angle boundaries (figure 1a) and crystallites with high-angle boundaries (figure 1b). Inserted in fig. 1b micro-diffraction pattern argues for high angle boundaries formation in the area. After four DCAP cycles mix structure contains recrystallized grains with the absence of dislocations and the crystallites with high-angle grain boundaries (figure 1c).The average size of structural fragments is 500-600 nm in A3003 alloy after DCAP. In the A7075 alloy two cycles of DCAP leads to stronger structural refinement. Figure 2 demonstrates UFG structure with high dislocation density and non-equilibrium high-angle boundaries. The average grain size in this case is 200 nm.

2.2. Mechanical testing

For tensile testing, flat specimens with a gage length of 17 mm, thickness of 0.5 mm and width of 6 mm machined from both as received and DCAP processed bars were pulled to failure using a ZWICK/RoellZ050 testing machine at a strain rate of 2 10^{-3} s^{-1}. The specimens were prepared and tested according to ASTM 8/E-8M-08.

Cylindrical samples with lengths of 4 mm and diameters of 7 mm were machined from both the as received and DCAP processed bars. The longitudinal axis of the specimens coincide with the pressing direction of the bars. Than the specimens were compressed dynamically at split Hopkinson pressure bar at strain rate in the range of 3.5-6.6 10^3 s^{-1} using the procedure described in [13, 14]. At least three specimens were tested under the same experimental conditions. The stress -σ, and strain-ε, were determined in-situ during dynamic loading based on elastic pulses in input and output measuring bars using the relationships presented in [13].

During dynamic compression, the surface temperature of the specimens was detected with a FLIP SC 5000 infrared camera. The spatial resolution of the camera is 0.2 mm, the temperature sensitivity is 0.025 K, the recording frequency is 3 kHz. Under dynamic loading conditions, the heat losses due to

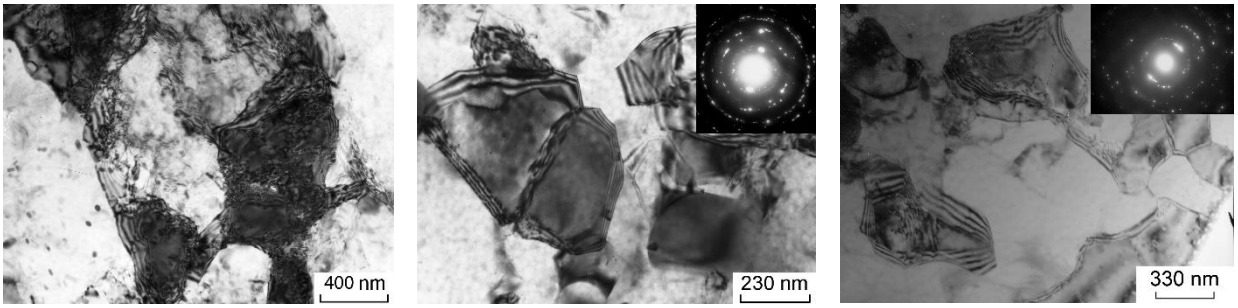

a b c

Figure 1. Structure of the DCAP-1 A3003 (a, b) and the DCAP-4 A3003 alloys (c).

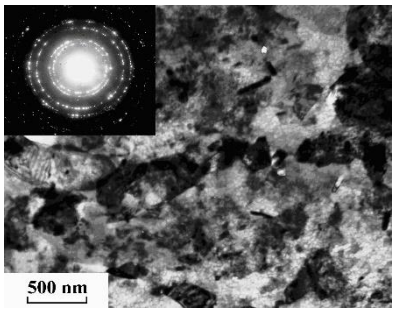

Figure 2. Structure of the DCAP-2 A7075 alloy.

exchange with the environment are negligible. Therefore, based on the temperature evolution data during compression, the fraction of dissipated energy was determined as

$$\beta = E_2 / E_1 ,$$

where E_1 - is the energy consumed for specimen deformation, E_2 - is the energy converted into heat due to deformation [14].

For shock-wave experiments disc shaped specimens with the thickness of 2 mm were machined from the as received and DCAP processed bars in such a way that longitudinal axis of the specimens coincide with the pressing direction of the bars. The specimens were loaded by the stroke of a flat aluminum plate ~0.4 mm thick, which was accelerated to a velocity of 630±30 m/s using explosive devices [1, 2].The experimental scheme is shown in figure 3. Under the given loading conditions, the pressure of the impact compression was 4–5 GPa. The deformation rate varied from 1.2 10^5 to 1.6 10^5 s^{-1}. Velocity of the back free surface of the specimens - $u_{fs}(t)$ was recorded by means of VISAR laser Doppler velocimetry [15] with a time resolution of ~1 ns.

The Hugoniot elastic limit σ_{HEL} and the yield stress Y were calculated from the elastic precursor front amplitude u_{fsHEL} according to velocity profiles as follows:

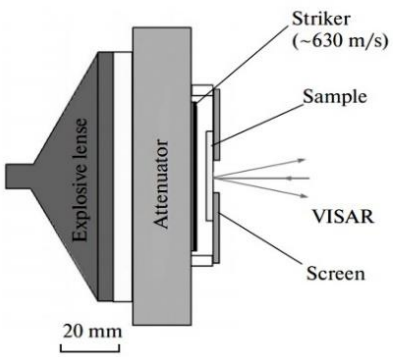

Figure 3. The scheme of the shock-wave loading experiment.

$$\sigma_{HEL} = \rho_0 c_l u_{fsHEL}/2$$

$$Y = \frac{1-2\nu}{1-\nu}\sigma_{HEL} = 2\sigma_{HEL}\left[\frac{c_s^2}{c_l^2}\right] \cong 1.5\sigma_{HEL}\left(1-\frac{c_b^2}{c_l^2}\right),$$

where ρ_0 is the initial density of the material, C_b, C_l, C_s– are the bulk, longitudinal, and shear sound velocities in material respectively, ν – Poisson's ratio.

Consider an allowance due to elastic–plastic behavior of the investigated materials -δ, the spall strength - σ_{sp} was determined from the following relation [1]:

$$\sigma_{sp} = 1/2\,\rho_0 c_b(\Delta u_{fs} + \delta),$$

Where Δu_{fs} is a drop of the velocity from the maximum to the first minimum due to the formation and propagation of reflection wave.

Material microhardness H was determined by means of indentation on PMT-3 facility with the load of 0.2 N. The measuring error did not exceed 10%. Brinell hardness test at a load of 250 kg with a 10 mm diameter ball was used to measure hardness of the alloys.

2.3. Microstructural characterization

The grain structure of the alloys was examined using Philips CM-30 transmission electron microscope (TEM) operating at an accelerating voltage of 200 kV. The average size of structural fragments was calculated based on dark-field images using the SIAMS image analysis software. The X-ray diffraction (XRD) analysis was performed on a DRON-3 diffractometer using CoK_α radiation. The Profile software was used to process the data by the approximation method and to calculate a root-mean square lattice microstrain $\langle\varepsilon^2\rangle^{1/2}$, crystal lattice parameter – a, and the size of coherent scattering region (D_{CSR}). Dislocation density was determined from the following relation:

$$\rho_d = \frac{2\sqrt{3}\left\langle\varepsilon^2\right\rangle^{1/2}}{\left(D_{CSR} \times b\right)},$$

where $b = a\sqrt{2}/2$ is Burgers vector for fcc metals.

3. Results

3.1. Dynamic compression at split Hopkinson pressure bar

Figures 4a, b shows stress-strain curves for DCAP-2 A7075 alloy and for DCAP-1 A3003 alloy obtained at different strain rates in a range of 3.5-6.6 10^3 s^{-1}. For the DCAP-2 A7075 alloy, the anomalous (inverse) dependence of yield stress on strain rate is established. There is the decreasing of yield stress on 27% when strain rate changes from 4 10^3 s^{-1} to 6 10^3 s^{-1}. Contrary, for DCAP-1 A3003 the increasing of yield stress is observed with increasing of strain rate, the same as for coarse-grained

alloys (figure 4c). Comparing with coarse grained materials the yield stress of DCAP-2 A7075 alloy is by 20% lower and of DCAP-1 A3003 alloy is by 28% higher at the same strain rate about 6 10^3 s^{-1}. For the DCAP-1 A3003 alloy, the strengthening effect in reference to CG state also depends on strain rate. Thus, yield strength is increased by 47% at strain rate of 4 10^3 s^{-1}against 28 % at strain rate of 6 10^3 s^{-1}, when compare with coarse-grained alloy. The yield stress value reaches 260 MPa and 280 MPa at low strain rate, and reaches 190 MPa and 295 MPa at high strain rate for UFG alloys A7075 and A3003 respectively.

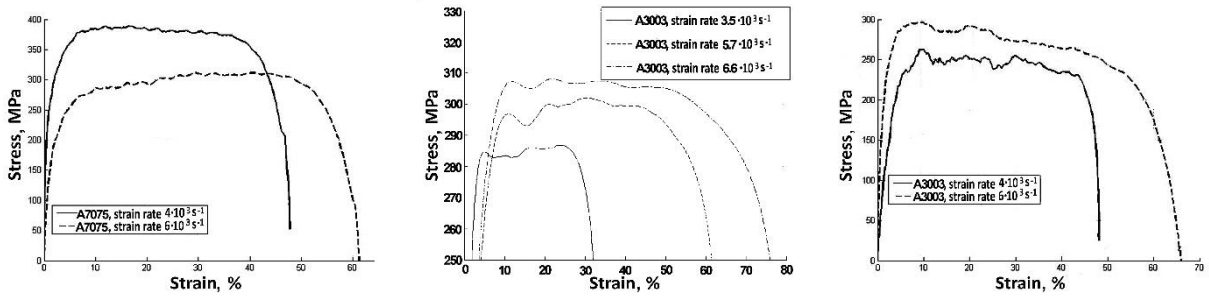

a b c

Figure 4. Stress-strain curves for UFG DCAP-2 A7075 alloy (a), UFG DCAP-1 A3003 alloy (b) and for CG A3003 alloy (c) at different strain rates.

To qualify dissipation capability of different alloys the values of dissipated energy ratio were compared at different strain rate [16]. It can be seen from figure 5, that the amount of dissipated energy is different for alloys in the UFG state having different structures and in the CG state. For instance, DCAP-2 A7075 and DCAP-1 A3003 alloys dissipate more elastic energy then the CG alloys respectively, but DCAP-4 A3003 alloy, conversely, dissipates less energy than the CG alloy at all investigated strain rates. The comparison of dissipated energy ratio of UFG A3003 alloy with two distinct types of structure shows that alloy with recrystalizated grains dissipates less and stores more energy. Energy dissipation capability of UFG DCAP-1 A3003 alloy does not depend on strain rate. However, for UFG DCAP-2 A7075 alloy the increasing of strain rate from 4 10^3 s^{-1} to 6 10^3 c^{-1} results in the growth of dissipated energy ratio from 0.62 to 0.8.

3.2. Shock wave loading

The strength properties of the DCAP-1, DCAP-2, and CG A3003 and A7075 alloys at a strain rate of (1.2-1.6) 10^5 s^{-1} are set out in a table 1, where σ_{HEL} is a Hugoniot elastic limit; Y is a dynamic yield strength; σ_{sp} is a spall strength.

Table 1. Dynamic strength properties of UFG and CG alloys.

Material	σ_{HEL}, GPa	Y, GPa	σ_{sp}, GPa
DCAP-2 A7075	0.42	0.21	1.32
CG A7075	0.28	0.14	1.38
DCAP-1 A3003	0.34	0.18	1.34
CG A3003	0.25	0.13	1.25

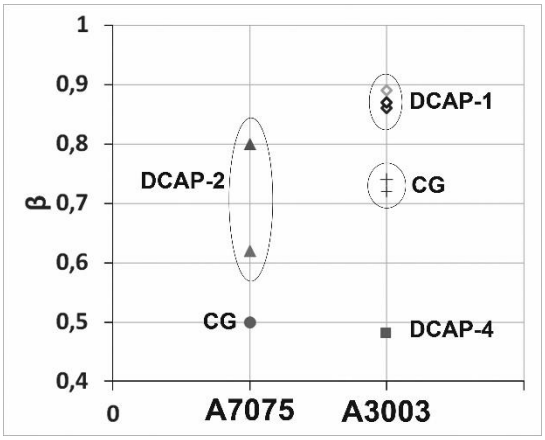

Figure 5. Dissipated energy ratio for A7075 and A3003 alloys at different strain rates.

It was shown that for DCAP-2 A7075 alloy Hugoniot elastic limit is by 50% greater than that for CG alloy, for DCAP-1 A3003 alloy σ_{HEL} is greater that for the CG one by 35%. The same changes are observed for dynamic yield strength. Spall strength is the same for DCAP-2 and CG alloy A7075, but for DCAP-1 A3003 alloy spall strength is increased by 7% in comparison with CG alloy.

Figure 6 demonstrates the dependence of yield strength on strain rate in a wide range of strain rates of 2 10^{-3}-1.6 10^{5} s^{-1}. Coarse-grained alloys strengthen up to strain rate in a range of 10^{3}-10^{4} s^{-1}. The same trend was observed for UFG A3003 alloy. Then alloys undergo softening at a strain rate about10^{5} s^{-1}. The dynamic yield strength, obtained at the strain rate about 10^{5} s^{-1}, is approximately the same as the yield strength at static conditions. The UFG A7075 alloy exhibits different and complicated behavior. Thus, the yield strength decreases at dynamic conditions compared with static conditions. The slight increasing of yield strength by 30 MPa is observed at strain rate 10^{5} s^{-1}. The comparison of the yield strength determined during static tensile tests and shock wave loading shows that the increment of the strength in regard to coarse grained alloy in the case of UFG A7075 alloy is 107% at static conditions and is 50 % in dynamics. In the case of UFG A3003 alloy the increment is 55% at static conditions and is 38% at dynamic conditions.

4. Discussion

The key attribute that distinguish DCAP from other static severe plastic deformation techniques is the superposition of several deformation modes of compression and tension due to the circulation of shockwaves and rarefaction waves and of the simple shear. Such complicated loading in combination with high strain rate promotes effective structural refinement upon 1-2 cycles of dynamic pressing and enhances significantly strength and hardness of alloys [10-12]. According to XRD analysis dislocation density increases by an order of magnitude and reaches the value more than 10^{15} m^{-2}. It is known, that evolution of ensembles of structural defects such as dislocation nucleation, sliding, interaction and annihilation is governed by strain rate. Therefore, the high level of internal stress can be explained by escalation of dislocation mobility as well as dislocation density due to activation of additional sliding systems [17]. Experimentally reviled peculiarities of structural formation during DCAP of aluminum alloys were confirmed completely by modeling of the process of high strain-rate deformation of metals using the equations of mechanics of continuum media containing defects [18].

It was established earlier that different structural states were formed depending on chemical composition of the alloy and DCAP mode [10-12, 19, 20]. Structures after DCAP of investigated alloys are shown in figure 1 and figure 2. The distinctive characteristics of the structural states are grain-subgrain size, dislocation density, proportion of high-angle and low-angle boundaries. It was determined that the non-equilibrium ultrafine-grained structure with high dislocation density of 2 10^{15} m^{-2} was formed in the DCAP-2 A7075 alloy.

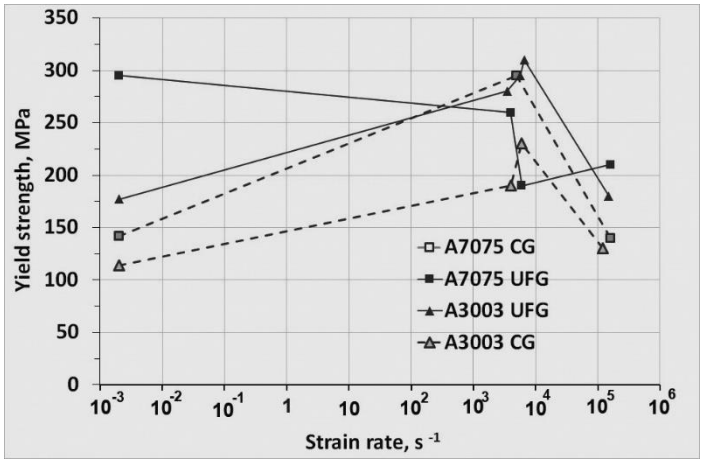

Figure 6. Strain rate dependence of yield strength of the DCAP-2 A7075 and the DCAP-1 A3003 and CG alloys.

The less defective mix UFG structure was formed in DCAP-4 A3003 alloy. The dislocation density in the DCAP-4 A3003 alloy is by an order of magnitude lower than in the DCAP-2 A7075 alloy. Since the main origin of internal stress is dislocation low-angle boundaries and disclinations in triple points [21], than the value of stored energy during DCAP will be different for the UFG A7075 and A3003 alloys. Structural evolution under further deformation is governed by the value of stored energy and connected with the relaxation of the internal stress. Thus, two different scenarios of the evolution of the structure during dynamic compression were observed for two investigated alloys at strain rate (3.5-6.6) 10^3 s^{-1}. The analysis of TEM images showed [16] that the grain-subgrain size maintains, well-developed dislocation substructure is formed and new low-angle boundaries appear in the DCAP-4 A3003 alloy after dynamic compression. Thus, the energy of dynamic compression was expend in the accumulation of the defects in the structure and therefore the increasing of stored energy was observed. Quite the opposite, non-equilibrium grain boundaries transform to more equilibrium state, the reduction of general dislocation density occurs in the DCAP-2 A7075 alloy. The evolution of the structure of the DCAP-2 A7075 alloy showed the activation of internal stresses relaxation processes. Transition electron microscopy data are complimented by XRD analysis. Due to dynamic compression of DCAP-2 alloy the root-mean square lattice microstrain was reduced from 0.17% to 0.12%, hardness was decreased by 300 MPa. The structure of DCAP-1 A3003 alloy responds the same way as DCAP-2 A7075 alloy. Consider that the less the proportion of stored energy than the more energy transforms in to heat, the ratio of dissipated energy of DCAP-2 A7075 alloy is 80 %, of DCAP-1 A3003 is 86%, and of DCAP-1 A3003 is 48% at strain rate 6 10^3 s^{-1}.

Irrespectively from chemical composition, a cell submicrocrystalline deformed structure was formed in the coarse grained alloys during dynamic compression. Furthermore, the root-mean square lattice microstrain increased and hardness grew by 200 MPa. Therefore, the part of the compression energy is consumed for defect formation due to that the proportion of stored energy increases.

DCAP UFG alloys possess higher hardness than CG alloys. Hardness increment is 700 MPa for DCAP-2 A7075 alloy and is 450 MPa for the DCAP-1 A3003 alloy. If there is no phase transformations than a strength and hardness increases due to grain boundaries length increasing and dislocation hardening. Comparison of the static mechanical properties have shown that yield strength and tensile strength of DCAP-2 alloy A7075 is 2 times higher and of the DCAP-1 A3003 alloy 1.5 times higher than of coarse grained alloys respectively. The difference of yield strength strongly depends on strain rate in the range of 10^3 s^{-1}. Mechanical behavior of UFG alloys under dynamic compression at strain rate of 10^3 s^{-1} is connected with structural evolution, which was described earlier. Thus, for CG alloys as well as for DCAP-1 A3003 alloy we observed normal (direct) yield strength-strain rate dependence, when for DCAP-2 A7075 alloy the inverse strain-rate dependence of the yield

strength was established (figure 6). Such anomalous behavior testify, that the deformation mechanism changes from dislocation sliding in CG alloy for grain boundary sliding for UFG A7075 alloy.

Under shock-wave loading the decreasing of deformation resistance was observed for both investigated UFG alloys against the strain rate of 10^3 s^{-1}. However, according to the table 1 [20] and figure 6 the dynamic characteristic of elastic-plastic transition is higher for UFG alloys than for CG alloys under shock-wave loading condition.

5. Conclusions

It was established that UFG A3003 alloy exhibits higher yield strength against CG alloy at a wide strain rate range from 2 10^{-3} to 1.5 10^5 s^{-1}. The UFG alloy A7075 undergo softening as regards to CG alloy at strain rate of (4-6) 10^3 s^{-1}. At this strain rates the alloy have inverse yield strength-strain rate dependence. At shock wave loading condition spall strength of both A3003 and A7075 UFG alloys is not poorer than of their CG analogs. Energy dissipation capability of UFG DCAP aluminum alloys is higher than of coerce grained alloys in the event that nonequilibrium heavily deformed structure is formed.

Acknowledgments

The work was performed in the framework of the state assignment of Russian Federal Agency for Scientific Organizations (theme “Structure”, no. 01201463331).

The authors thank the administration of the UrFU for access to the scientific equipment of the UrFU, supported by program 211 of the Government of the Russian Federation (agreement no. 02.A03.21.0006).

The electron-microscopic studies were performed at the Center of Collaborative Access “Testing Center of Nanotechnology and Advanced Materials, M. N. Miheev Institute of Metal Physics, Ural Branch, Russian Academy of Sciences.

References

[1] Antoun T, Curran D R, Razorenov S V, Seaman L, Kanel G I and Utkin A V 2003 *Spall Fracture* (New York: Springer) p 404

[2] Kanel G I, Razorenov S V and Fortov V E 2004 *Shock-Wave Phenomena and Properties Condensed Matter* (New York: Springer) p 321

[3] Razorenov S V, Garkushin G V, Kanel G I and Ignatova O N 2012 *Physics of the Solid State* **54**(1) 790-7

[4] Garkushin G V, Razorenov S V and Kanel G I 2008 *Technical Physics. The Russian Journal of Applied Physics* Effect of structural factors on submicrosecond strength of D16T aluminum alloy **53** 11 pp 1441-1446

[5] Razorenov S V, Kanel G I and Fortov V E 2003 *The Physics of Metals and Metallography* **95**(1) 86-91

[6] Shtremel M A 2012 *Russian metallurgy (Metally)* **10** 843-52

[7] Evstifeev A D, Gruzdkov A A and Petrov Y V 2013 *Technical Physics. The Russian Journal of Applied Physics* **58**(7) 989-93

[8] Borodin E N and Mayer A E 2012 *Physics of the Solid State* **54(**4) 808-15

[9] Borodin E N, Petrov Y V, Mayer A E and Gruzdkov A A 2014 *Physics of the Solid State* **56(**12) 2470-9

[10] Brodova I G, Shirinkina I G, Antonova O A, Shorokhov E V and Zhgilev I I 2007 *Materials science and engineering* **503**(1-2) 103-5

[11] Petrova A N, Shirinkina I G, Shorokhov E V, Minaev I V, Zhgilev I N and Abramov A V 2010 *Reviews on Advanced Materials Science* **25**(2) 128-35

[12] Shirinkina I G, Petrova A N, Brodova I G, Pilyugin V P and Antonova O A 2012 *The Physics of Metals and Metallography* **113**(2) 170-5
[13] Kolsky H 1949 *Proc. Phys. Soc* **62B** 676-700
[14] Plekhov O, Naimark O, Chudinov V and Leontev V 2009 *Technical Physics Letters* **35**(1) 92-5
[15] Barker L M and Hollenbach R E 1972 *Journal of Applied Physics* **43** 4669–75
[16] Petrova A N, Brodova I G, Plekhov O A, Naimark O B and Shorokhov E V 2014 *Technical Physics. The Russian Journal of Applied Physics* **59**(7) 989-96
[17] Meyers M A and Murr L E 1981 *Shock Waves and High-Strain-Rate Phenomena in Metals* (NewYork: Plenum Press) p 1101
[18] Borodin E N and Mayer A E 2013 *Technical Physics. The Russian Journal of Applied Physics* **58**(8) 1159-1163
[19] Petrova A N, Brodova I G and Razorenov S V 2017 *Physics of Metals and Metallography* **118**(6) 601–7
[20] Brodova I G, Petrova A N, Razorenov S V and Shorokhov E V 2015 *The Physics of Metals and Metallography* **116**(5) 519-26
[21] Koneva E V, Popova N A, Ignatenko L N and Pekarskaya E E 2000 *Investigation and applications of severe plastic deformation* (New York: Kluwer Acad. Publ.) 121-6